# Mechanism of the active divertor flux control by the supersonic-molecular-beam-injection with LHW-induced magnetic perturbations on the EAST tokamak

S.  $Xu^{1,2,3*}$ , M. Rack<sup>3,4</sup>, Y. Liang<sup>1,3,5†</sup>, M. Jia<sup>1,3</sup>, D. Reiter<sup>3</sup>, Y. Feng<sup>6</sup>, J. Cosfeld<sup>3</sup>, Y. Sun<sup>1</sup>, L. Wang<sup>1</sup>, W. Feng<sup>1</sup>, S. Liu<sup>1</sup>, B. Zhang<sup>1</sup>, X.L. Zou<sup>7</sup>, J. Huang<sup>1</sup>, J. Wu<sup>1</sup>, J. Xu<sup>1</sup>, L. Meng<sup>1</sup> and the EAST team

E-mail: \*s.xu@fz-juelich.de and †y.liang@fz-juelich.de

**Abstract.** The redistribution of the divertor flux caused by the synergy of the supersonic-molecular-beaminjection (SMBI) and the magnetic perturbations induced by lower hybrid waves (LHWs), has been observed on the Experimental Advanced Superconducting Tokamak (EAST) [Li J. et al 2013 Nature Phys. 9 817]. To reveal the physical mechanism behind, first simulations with good agreements to the experimental findings are performed by utilizing a self-consistent fluid 3D edge plasma Monte-Carlo code coupled to a kinetic neutral particle transport code. The ions and electrons originating from the ionization of injected neutral particles in the plasma edge flow along the magnetic flux tube towards to the divertor, thus directly increasing the divertor flux on the split strike lines in the footprint. Combining this with the multi-lobe structure of the edge magnetic topology, actively controlling the divertor flux can be realized by adjusting the SMBI position or the phase of the magnetic perturbations.

Keywords: particle and heat flux, magnetic topology, lower hybrid waves, supersonic molecular beam injection, edge plasma transport

<sup>&</sup>lt;sup>1</sup> Institute of Plasma Physics, Chinese Academy of Sciences, Hefei 230031, People's Republic of China

<sup>&</sup>lt;sup>2</sup> University of Science and Technology of China, Hefei 230026, People's Republic of China

<sup>&</sup>lt;sup>3</sup> Forschungszentrum Jülich GmbH, Institut für Energie- und Klimaforschung-Plasmaphysik, Partner of the Trilateral Euregio Cluster (TEC), 52425 Jülich, Germany

<sup>&</sup>lt;sup>4</sup> JARA-HPC, Jülich Supercomputing Centre, Forschungszentrum Jülich GmbH, 52425 Jülich, Germany

School of Electrical and Electronic Engineering, Huazhong University of Science and Technology, Wuhan, 430074, People's Republic China

<sup>&</sup>lt;sup>6</sup> Max-Planck-Institute für Plasmaphysik, 17491 Greifswald / 85748 Garching, Germany

<sup>&</sup>lt;sup>7</sup> CEA, IRFM, F-13108 Saint-Paul-lez-Durance, France

#### 1. Introduction

Confining a plasma by utilizing magnetic fields into an annular vessel known as a tokamak is one of the most promising approaches to generate controllable nuclear fusion power for human kind. A serious challenge for high-power long-pulse operations of the tokamak is how to prevent damage to the plasma-facing components by particles from the edge plasma. As an essential exhaust system for manipulating power flow and removing reaction wastes, the divertor has to resist giant heat load transported by the edge plasma flows from the core plasma. However, in the high-confinement mode (H-mode) operating scenario [1] of a future fusion device, such as ITER, the local heat deposition on divertor targets is quite high compared to the tolerance of the current materials, particularly during the edge-localized mode (ELM) crash which is kind of a magneto-hydrodynamic instability due to quasi-periodic relaxation of the edge transport barrier [2]. Therefore, actively controlling the divertor flux by feasible mechanisms is an attractive and significant topic for current tokamaks, as well as future fusion reactors.

Significant progress has been made in this research area in the past decades. As an effective measurement, resonant magnetic perturbations (RMPs) created by external magnetic coils have been demonstrated for causing the strike line splitting on divertor targets in many tokamaks [3–10]. They could also be used to ELM control through affecting the plasma pressure gradient and an associated current density in the edge plasma due to the changes of the magnetic topology. Nevertheless, an inevitable problem for applying coil-induced RMPs is that the plasma configuration is restricted in a narrow resonant edge safety factor window because of the fixed coil geometry. Fortunately, an alternative method has been found in experiments from the Experimental Advanced Superconducting Tokamak (EAST) [11]. Lower hybrid waves (LHWs), which were initially designed for driving a core plasma current by providing low momentum injection via electron Landau damping [12], can generate the similar magnetic perturbation effects by inducing helical current filaments flowing along magnetic field lines in the scrape-off layer (SOL) [13]. The helicity of current filaments always closely fits the pitch of the edge field lines whatever the edge safety factor is, so the spectrum of LHW-induced perturbation fields is adjusted automatically in different plasma configurations. Previous experiments and simulations indicated that such magnetic perturbations not only can be applied for ELM control as well, but also always have a good resonant effect with the dominant toroidal mode number n = 1, thus resulting in the strike line splitting on divertor targets [14].

Recently, a potential actuator to control the divertor flux distribution by using the synergy of the supersonic-molecular-beam-injection (SMBI) [15] and LHW-induced magnetic perturbations has been observed on EAST experiments [16]. This measurement has already been

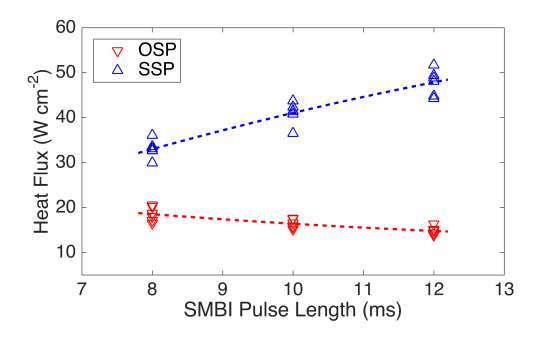


**Figure 1.** (color online). The heat flux measured by an infrared camera at the OSP and the SSP of a toroidal position on the lower outer divertor in the H-mode discharge #41810 with various SMBI pulse lengths, i.e. 8, 10, and 12 ms

utilized to help EAST achieve a new record duration of steady-state H-mode discharge over 100 seconds in the 2017 campaign [17]. However, the physical mechanism behind is still not clear.

In this paper, we report on the first simulations along with above experimental observations performed by utilizing the self-consistent fluid 3D edge plasma code EMC3 [18] coupled to the kinetic neutral particle transport code EIRENE [19, 20]. EMC3 solves a set of Braginskii fluid equations formulated in a Fokker-Planck scheme by using the Monte-Carlo method, while the EIRENE code is for multi-species Boltzmann equations with chemical processes, based on conventional Monte-Carlo particle transport algorithms. After continuous improvements and upgrade in the past years, EMC3-EIRENE now is capable of taking into account the LHW-induced magnetic perturbations with both the physical and geometrical effects being considered [21].

## 2. Experimental observations

EAST is the first fully superconducting tokamak device built for demonstrating the long-pulse stable high-performance plasma with ITER-like heating schemes, i.e., dominated by electron heating from LHWs, neutral beam injection (NBI), ion cyclotron resonance heating (ICRH) and electron cyclotron resonance heating (ECRH). At present, two LHW systems operating at frequencies of 2.45 GHz and 4.6 GHz respectively, and two SMBI systems designed initially for plasma density maintenance, are installed at the low field side mid-plane in different toroidal positions. Hereinafter, the toroidal angle  $\varphi$  of the device is defined by locating the center of the 4.6 GHz LHW antenna at  $\varphi = \pi$ , and the positive toroidal direction is anticlockwise direction from the top view.

The influence of SMBI pulses with LHW-induced magnetic perturbations on the divertor heat flux has been studied in a H-mode deuterium plasma discharge [22]. In this experiment, the plasma is predominantly driven by the

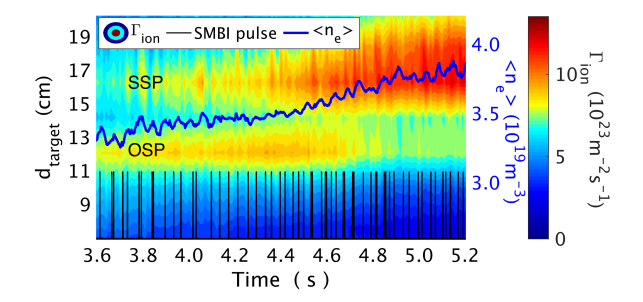


**Figure 2.** (color online). Time evolution of the parallel ion saturation current on the upper outer divertor in the discharge #64784. Here,  $d_{target}$  is the distance to the divertor corner marked in figure 4. The blue line belongs to the blue label  $< n_e >$  which is the line-averaged plasma density. The black vertical lines indicate the pulse time and the pulse length in this discharge, and the line height does not have a physical meaning.

2.45 GHz LHW system, with the SMBI pulse length being varied from 8 to 12 ms. The plasma-stored energy varied slightly (within  $\pm \sim 3\%$ ) following the SMBI pulse. The peak heat flux located at the split strike point (SSP) was increased immediately after each SMBI pulse, while the peak heat flux near the original strike point (OSP) was reduced. Then both of them reverted to their previous states. This divertor flux redistribution became more obvious with the increase in the SMBI pulse length as shown in figure 1. During the 2012-2014 shutdown, the material of the upper divertor on EAST has been upgraded from graphite to tungsten. Figure 2 shows that the distribution of the parallel ion saturation current measured by Langmuir probes on the divertor target is changed with the SMBI injection rate in a density ramp-up discharge (#64784) with an ITERlike tungsten divertor. The 4.6 GHz LHW system with ~0.9 MW was used in this upper single-null configuration discharge with a toroidal plasma current  $I_p \sim 0.4$  MA. In this figure, the SMBI injection rate is increased with the discharge time. After the ramped density caused by the SMBI reached a critical threshold (after ~4.4 s), the particle flux near the SSP location follows the increase in the plasma density, while the particle flux at OSP decreases.

## 3. Simulations

Such divertor flux redistributions caused by SMBI during the presence of magnetic perturbations have been investigated for the first time through a series of simulations by using the self-consistent EMC3-EIRENE code. In these simulations, an upper single-null configuration deuterium plasma with LHW-induced magnetic perturbations in the discharge #64784 at 4.15 s is utilized in generating a toroidal  $2\pi$  rad computational grid of the whole magnetic field. The total current of LHW-induced filaments is 2 kA with a distance ~28±8 mm to the last closed flux surface (LCFS) at the mid-plane in front of the LHW antenna. The

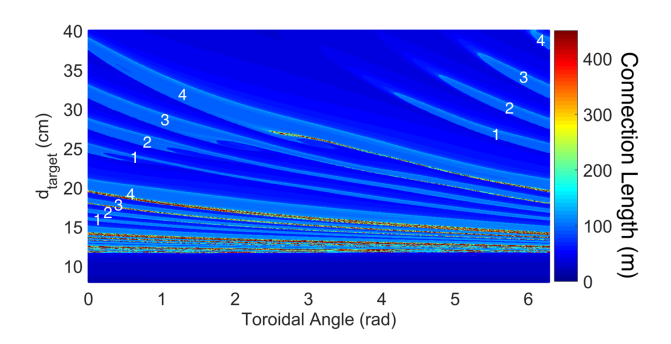


**Figure 3.** (color online). The connection length footprint on the upper outer divertor target with LHW-induced magnetic perturbations. The numbers with white color represent the serial number of split arms. The arms with the same serial number are the same arms, but in different toroidal loops.

formation of the filaments is the same with that in Ref. [21]. The positions and pitch angles of the filaments show a good agreement with the helical radiation belts observed by the visible camera. The input power  $\sim\!640$  kW provided from the experiment is assumed equally distributed between electrons and ions. Here, the power radiated by impurities has been subtracted from the total heating power, because the simulations are only for the deuterium plasma without considering impurities. The separatrix density is set at  $4\times10^{18}$  m<sup>-3</sup> based on the experiment. The constant anomalous cross field transport coefficient of particle  $D_\perp$  is determined as 0.2 m<sup>2</sup>/s by fitting the divertor probes at a fixed toroidal position [21,23]. The cross field energy transport coefficient  $\chi_\perp$  is assumed as  $5D_\perp$ , which agrees to previous simulations on EAST [21,24].

According to previous studies [14, 21], although the dominant toroidal mode number of LHW-induced perturbations is n = 1, the higher order perturbations also have obvious contributions to change the magnetic topology, thus leading to one split striation with some arms in the divertor footprint as shown in figure 3. The number of the arms is the same with the number of LHW antenna rows.

Figure 4(a) and (b) illustrate the particle and heat fluxes without the SMBI simulated by EMC3-EIRENE on the upper outer divertor with the diagnostic position marked. Both of the OSP and SSP positions show a good agreement with the experimental findings shown in figure 2. Similar to the magnetic field line footprint, one split striation with four arms is appeared in the divertor flux pattern. The pitch angles of these arms are consistent with those of magnetic field lines at the same locations. Therefore, they decrease with an increase in the edge safety factor  $q_{95}$ , namely, the angle between the split strike line and the original strike line on the divertor target decreases with an increase in the edge safety factor  $q_{95}$ . It should be mentioned that this angle is also related to the positions of the divertor target, and other plasma configuration

parameters.

After reproducing the background plasma, some experimental operating parameters about the SMBI should be configured as part of the following simulation inputs. The nozzle of the SMBI is ~2 m away from the plasma at mid-plane. Although the beam is ejected freely to the vacuum chamber without any guiding pipe, its divergence angle is only about five degree due to the high pressure of the source. In the following simulations, the particles from the SMBI are injected radially. The polar angle of source particles against the injected direction is sampled from a Gaussian distribution with zero as mean value, and the standard deviation of the distribution is three degree. The beam is formed by deuterium molecules with the initial temperature ~300 K. The injected velocity is sampled from a truncated Maxwellian density distribution shifted by a velocity of 1200 m/s. The injection rate is assumed as

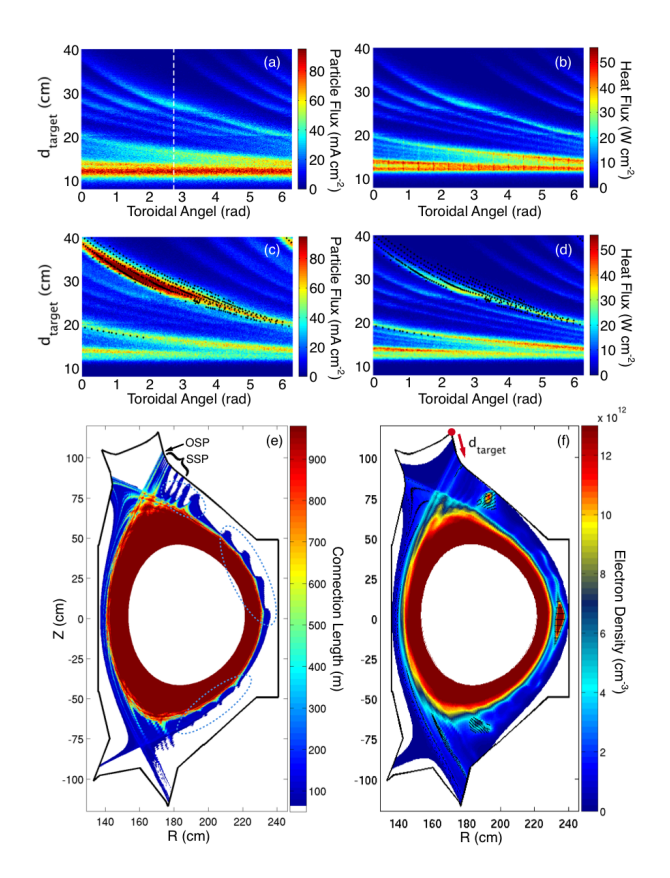


**Figure 4.** (color online). The simulated footprints of (a) particle flux and (b) heat flux without the SMBI on the upper outer divertor. The white dashed line in figure (a) corresponds to the position of the divertor Langmuir probes. Figure (c) and (d) show the simulated particle flux and heat flux with the SMBI on the same divertor. The poloidal cross-sections of (e) the connection length and (f) electron density at the same toroidal position with the SMBI. Here, the SMBI system is located at the midplane of the lower field side in a toroidal position of  $13\pi/8$  rad. Every dashed ellipse in figure (e) marks a group of the multi-lobe structure of the edge magnetic topology. The black points in figure (c, d, f) represent the positions of the field lines traced from the SMBI-induced higher density region. The red point in figure (f) corresponds to the divertor corner, which is used as a reference point in other figures.

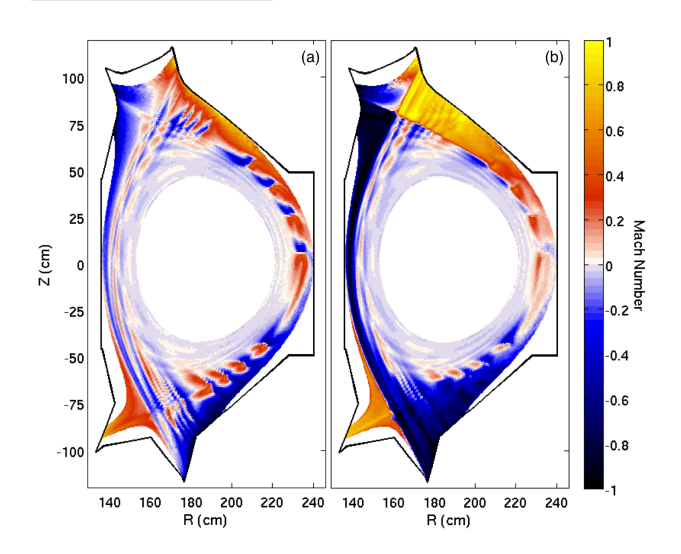


**Figure 5.** (color online). The poloidal cross-sections of the Mach number (a) without and (b) with the SMBI, respectively. The toroidal position is same with the SMBI system.

 $4.682 \times 10^{21}$  molecules s<sup>-1</sup> according to the experimental calibration [25].

The simulated particle and heat fluxes on the upper outer divertor during the SMBI with LHW-induced magnetic perturbations are redistributed as shown in figure 4(c) and (d), respectively. Similar to the experimental observations with the SMBI, both of them are decreased near the OSP location, while they are increased at the SSP position. Although previous numerical analyses indicate that the momentum loss in the edge island structure, and enhanced perpendicular energy transport may lead to the absence of the high recycling regime in divertor region during using magnetic perturbations [26, 27], the divertor flux on the OSP seems like to turn into a slight detached state with the increase in the plasma density. The realization of the detachment divertor regime [28] needs a sufficient upstream plasma pressure, enough input energy for the ionization process, as well as effective neutral confinement. The SMBI pulses with high speed not only provides substantial ionization source at the plasma edge within a short time, but also further affect the edge ion sonic-velocity  $v_{\parallel}$  and the parallel convection energy flux (~  $5/2nT_{i,e}v_{\parallel}$ ), thus causing the density regime modification. According to the simulations, the SMBI results in the 3D distribution changes of the plasma density n, temperature  $T_{i,e}$ , as well as the parallel flow velocity. Figure 5 presents the change of Mach number distributions caused by the SMBI.

One significant reason for the increase of the divertor flux at the SSP position, is discovered based on our simulations. Except for the interpretation presented in the Ref. [16] that the increased plasma density results in higher particle and heat fluxes from the core plasma by an additional LHW-induced transport channel, a higher density

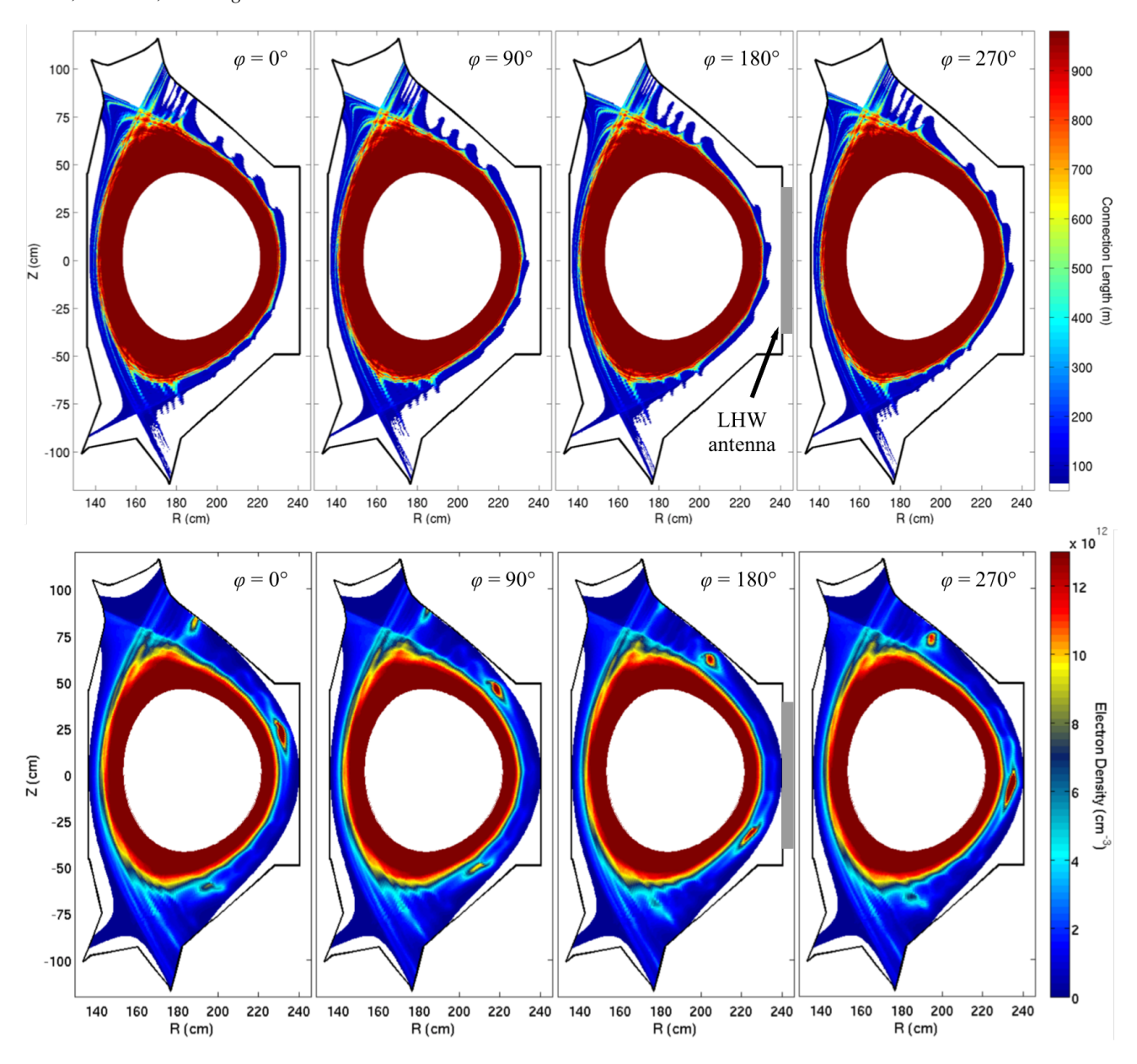
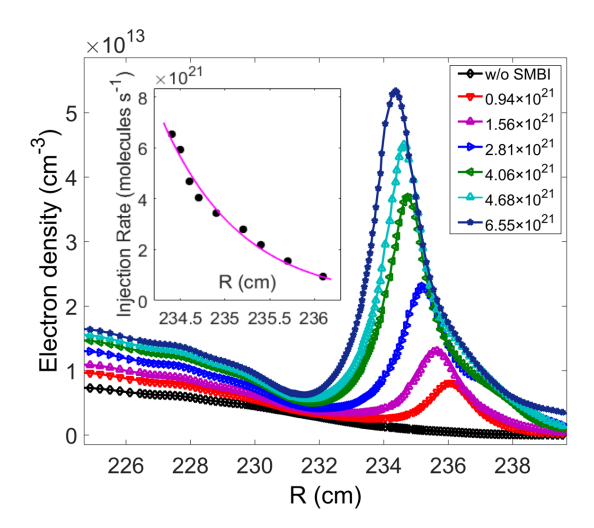


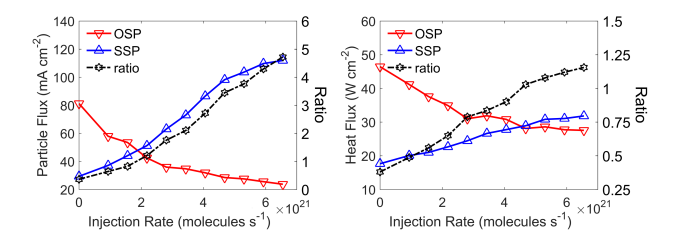
Figure 6. (color online). The 2D distributions of the magnetic field line connection length and the simulated plasma density at different toroidal positions.

flux tube formed by the SMBI with LHW-induced magnetic perturbations also plays an important role. Because of a small divergence angle, the injected molecule particles are ionized locally where the plasma temperature is larger than the ionization temperature threshold in the SOL. Here, the complex ionization processes are regarded in the EIRENE part based on the AMJUEL/HYDHEL database. A higher density region is formed in front of the SMBI system at the mid-plane as shown in figure 4(f). Due to much stronger parallel transport compared with cross field diffusion, through the field line tracing technique, it is found that the charged particles in this region flow along the magnetic flux tube towards the divertor, thus directly increasing the heat and particle flux on the split strike lines.

Wherein, the effect on the particle flux is more obvious than that on the heat flux because of the low temperature of these charged particles. The LHW-induced magnetic perturbations form the multi-lobe structure of field lines with a long connection length near the LCFS as shown in figure 4(e) [13, 14]. One of the lobes at the mid-plane is located in front of the SMBI system. In this lobe, with increasing plasma density and decreasing temperature the local collisionality becomes larger, and the cross-field energy conduction is enhanced. The charged particles caused by the SMBI can obtain more energy from the inner plasma in the lobe by the charge-exchange process and particle collisions, resulting in a higher heat flux at the SSP. To show the 3D effects of the multi-lobe structure,



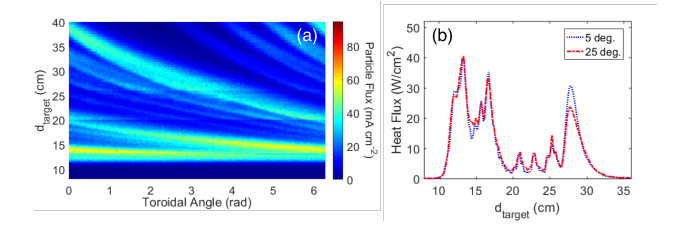
**Figure 7.** (color online). The radial density profile along the injected direction with different SMBI injection rates. The small plot indicates the radial position of the peak density in terms of the different injection rate of the SMBI.



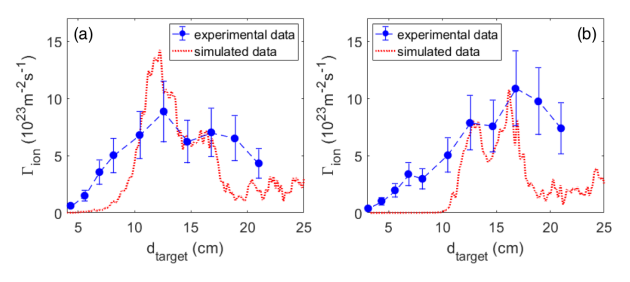
**Figure 8.** (color online). The changes of simulated divertor fluxes on the OSP and SSP with different SMBI injection rates at the toroidal positions marked in figure 4(a). Here, the parameter  $d_{target}$  of the OSP and the SSP are  $\sim$ 11.8 cm and  $\sim$ 27.3 cm, respectively.

figure 6 provides the 2D distributions of the magnetic field line connection length and the simulated plasma density at other toroidal positions. From the previous study [14], the effective perturbations from higher toroidal mode numbers are the main reasons to create the 3D multi-lobe structure.

It should be mentioned that the redistribution of the divertor flux caused by the SMBI is more obvious with an increase in the injection rate, which is indicated in both simulations and experiments. For the case of a higher SMBI injection rate, more injected particles and a deeper deposition depth of the local higher density region induced by the SMBI in the SOL bring more particle and energy sources for the interaction between plasma and injected particles. The deposition depth not only depend on the injection speed and the density profile for a given shot, but also depend on the injection rate. Figure 7 shows the radial density profile along the injected direction with different SMBI injection rates. The peak density position in the SMBI-induced higher density region in the SOL moves to the core direction with an increase in the injection rate, namely, more injected particles are deposited at the inner



**Figure 9.** (color online). (a) The simulated particle flux distribution on the upper outer divertor with the divergence angle of the SMBI as 25 degree. Other simulated parameters are the same with the simulation shown in figure 4(c). (b) The simulated heat flux distribution on the upper outer divertor with different divergence angles of the SMBI at a toroidal position of  $3\pi/4$ .



**Figure 10.** (color online). The profiles of experimental and simulated parallel ion saturation current on the upper outer divertor target without the SMBI (a) and with the SMBI (b), respectively. The toroidal measurement position of divertor Langmuir probes has been marked in figure 4(a).

region of the LHW-induced multi-lobe structure where has higher plasma temperature. Thus more energy sources are provided to the interaction between plasma and injected particles. With assuming a constant perturbation field, similar to the experimental observations, figure 8 shows the simulated result that the ratio between the peak divertor flux on the SSP and the OSP is enhanced with the increased SMBI injection rate.

The divergence angle of the SMBI also has an evident influence on the divertor flux distribution. Figure 9 presents the simulated divertor flux with a higher divergence angle as 25 degree and the standard deviation as 15 degree. Although this assumption cannot be realized in the present experiments on EAST, the results may be good for understanding the physics behind better. Combining with figure 4(a), the simulations show that with a constant injection rate and velocity, the effects of the divertor heat flux control are better with a smaller divergence angle of the SMBI. Note that the simulated results except for figure 9 are performed using the divergence angle as 5 degree, which is consistent with the experimental calibration.

In addition, a higher plasma density caused by the SMBI in the SOL may absorb more LHW power and increases LHW-induced magnetic perturbations, thus further affecting the distribution of the divertor flux. According to EAST experiments, the plasma density has an evident effect on the LHW absorption [29]. The current

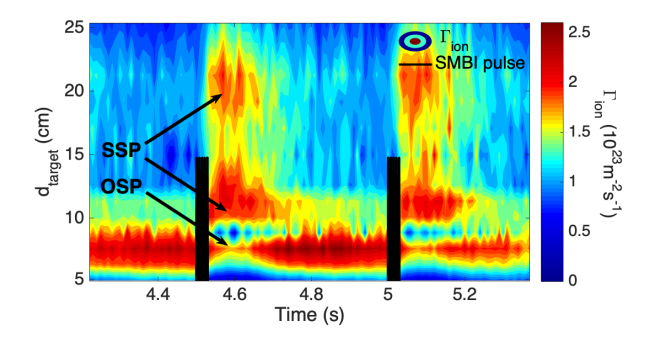


**Figure 11.** (color online). Time evolution of the parallel ion saturation current measured by Langmuir probes on the upper outer divertor in the Ohmic discharge #85791 without using magnetic perturbations. Similar to figure 2, The black vertical lines indicate the pulse time and the pulse length.

amplitude of the LHW-induced helical current filaments increases with an increase in either the LHW input power or the plasma density [13, 21]. From figure 6, the SMBI-induced local higher density region is formed in front of the LHW antennas by flowing the magnetic flux tube, thus increasing the LHW absorption in the SOL. These absorbed energies not only further weakly increase the heat flux at the SSP on divertor targets, but also affect the amplitude of magnetic perturbations. However, so far the quantitative relationship between the LHW absorption, the SMBI and the LHW-induced magnetic perturbations is still unclear due to the complex physics processes. This need to further study from the experiments and simulations in the future.

For the quantitative comparison, figure 10 shows profiles of experimental and simulated parallel ion saturation current on the upper outer divertor target. It shows an agreement between the simulation and the experiment. The discrepancy may be caused by undetermined deviations from experimental measurements, the estimated LHW-induced SOL filament current, the deviation of the SMBI conditions, non-uniform cross field transport coefficients and so on. The impurity effects also is a reason of the absolute value discrepancy, which has been discussed in the Ref. [30].

The prediction of the local higher density region induced by the SMBI has been verified in the EAST experiments. So far, there is no diagnostic which can directly provide the density profile in the simulated higher density region in the SOL on EAST, because of the quite limited number of diagnostics at distinct locations with different plasma positions. However, according to the simulations, if a higher density region caused by the SMBI is formed in the SOL, the split strike points should be measured by the divertor probes in an Ohmic discharge without magnetic perturbations, because the plasma in such higher density region will flow along the magnetic flux tube towards to the divertor. Recently, such experiments have demonstrated on EAST to verify that the SMBI actually generated a local higher density region in the SOL.

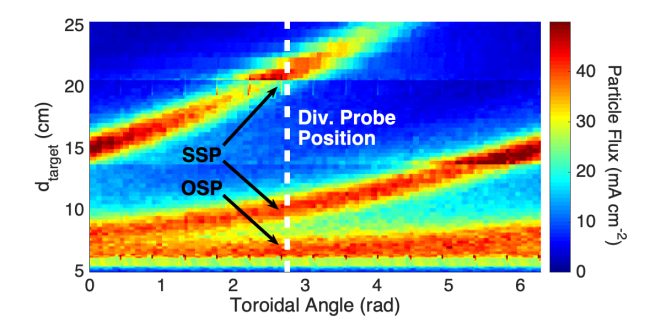


**Figure 12.** (color online). The simulated particle flux on the upper outer divertor with the SMBI in the Ohmic discharge #85791 without using magnetic perturbations. The white dashed line corresponds to the toroidal position of the divertor Langmuir probe.

In the experiment without magnetic perturbations (EAST #85791), the SMBI only injected several pulses in order to show clearly its effects on the divertor flux. Figure 11 indicates the parallel ion saturation current measured by the divertor probes in the Ohmic discharge #85791 with upper single-null configuration ( $I_p \sim 0.4$  MA,  $q_{95} \sim$ 6.05). The split strike points are appeared as predictions after each SMBI pulse. Figure 12 shows the simulated particle flux on the divertor target using the EMC3-EIRENE code. The split strike point caused by the SMBI-induced local higher density region shows a good agreement with the experimental data. In the Ohmic discharge without magnetic perturbations, there is no evident split strike line for the divertor heat flux caused by the SMBI both from the experiment and the simulation. This further proves that the divertor flux control is benefit from the synergy of the SMBI and the magnetic perturbations.

Utilizing the multi-lobe structure of the magnetic topology with the density feedback control by the SMBI, a method to actively steer the divertor flux is proposed by adjusting the SMBI position or the phase of magnetic perturbations. The SMBI system in the above #64784 discharge simulations is located at the toroidal position of  $13\pi/8$  rad. Owed to the strong three-dimensional feature of the magnetic topology with LHW-induced perturbations, it is worthy to simulate the edge plasma transport with another SMBI system (corresponding to the toroidal position of  $\pi/2$ rad) on EAST. The LHW-induced multi-lobe structure of the magnetic topology near the LCFS can be regarded as several groups. The number of lobes in each group is the same as the number of rows of the LHW antenna. From figure 4, the high plasma density region caused by the SMBI is located at the lowest lobe in a group of the multilobe structure. It results in that the largest modification of divertor flux appears in the highest split striation arm on the footprint. In contrast, if the SMBI position corresponds to the highest lobe in a group of the multi-lobe structure as shown in figure 13, the divertor flux modification located at the lowest split striation arm has the largest modification.

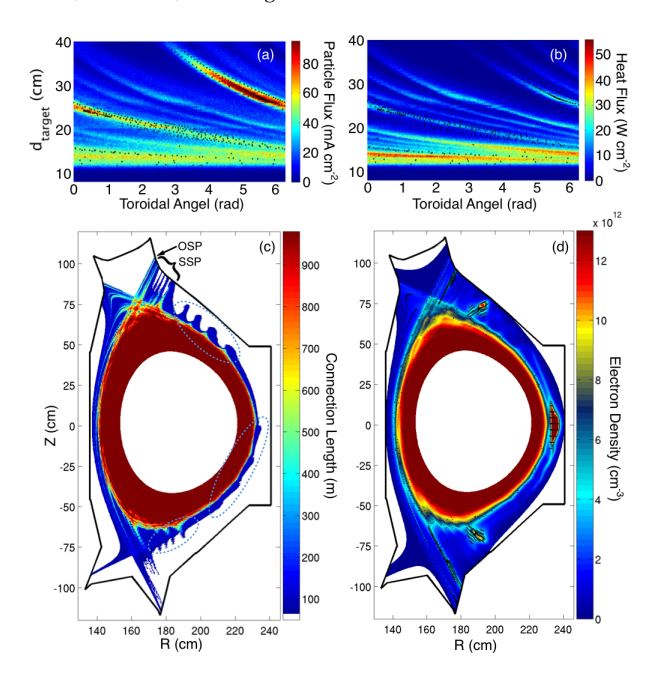


**Figure 13.** (color online). Same as figure 4, but in case of the SMBI system located at a toroidal position of  $\pi/2$  rad.

A more intuitive comparison is illustrated in figure 14. This method can be regarded as an actuator to control the deposited portions of plasma flow power among the split arms, thus averaging out the non-toroidally uniform erosion on the divertor target. It should be mentioned that, although the particle flux at the SSP are increased due to the SMBI, the energy of these particles is much lower than that of particles at the OSP without the SMBI according to the experiments and simulations. The damages of divertor targets at the SSP are also much weaker than that of divertor targets at the OSP without the SMBI. Note that, either SMBI or LHW-induced perturbations can achieve the ELM control by itself from past experiments. To further optimize the effectiveness of the divertor flux control in H-mode plasmas, more experiments with different SMBI conditions, LHW input power, and plasma edge safety factors, should be performed on EAST in the future.

# 4. Summary

In summary, the divertor flux redistribution caused by the synergy of the SMBI and LHW-induced magnetic perturbations on EAST has been reproduced for the first time in simulations by utilizing a self-consistent fluid 3D edge plasma Monte-Carlo code coupled to a kinetic neutral particle transport code. The results show that the local interaction between plasma and the injected particles in the plasma edge can be used to actively control the divertor flux. This benefits from the low divergence of the SMBI technique and the multi-lobe structure of edge magnetic

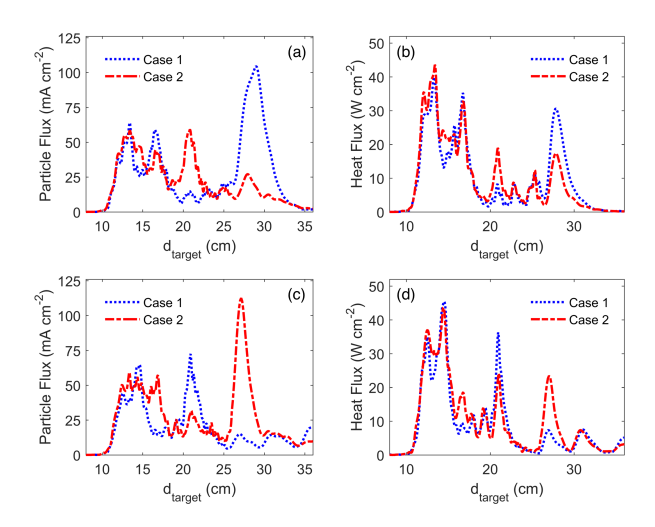


**Figure 14.** (color online). The 2D simulated divertor fluxes on the upper outer divertor at toroidal positions of (a, b)  $3\pi/4$  and (c, d)  $7\pi/4$ . The case 1 and case 2 correspond to the same SMBI toroidal positions with figure 4 and figure 13, respectively.

topology induced by LHWs. The method can also be applied to the case in which the 3D edge magnetic topology is induced by the RMP coils instead. These simulations will enlighten an attractive approach to actively optimize the heat load distribution on the targets, and to reduce the large transit peak divertor flux for next-step fusion devices.

# ACKNOWLEDGMENTS

This work is supported by the National Key R&D Program of China under Grant No.2017YFE0301100, K.C. Wong Education Foundation, and National Natural Science Foundation of China under Grant No. 11575236, No. 11875292, No. 11875294 and No. 51828101. The authors gratefully acknowledge Dr. F. Schluck for proofreading the paper, and the computing time granted by the JARA-HPC Vergabegremium and VSR commission on the supercomputer JURECA at Forschungszentrum Jülich.

### References

- [1] Wagner F. et al 1982 Phys. Rev. Lett. 49 1408
- [2] Zohm H. et al 1996 Plasma Phys. Control. Fusion 38 105
- [3] Evans T. et al 2006 Nat. Phys. 2 419
- [4] Liang Y. et al 2007 Phys. Rev. Lett. 98 265004
- [5] Kirk A. et al 2010 Nucl. Fusion **50** 034008
- [6] Suttrop W. et al 2011 Phys. Rev. Lett. 106 225004
- [7] Bécoulet H. et al 2014 Phys. Rev. Lett. 113 115001
- [8] Sun Y. et al 2016 Phys. Rev. Lett. 117 115001
- [9] Jia M. et al 2018 Nucl. Fusion 58 046015
- [10] Park J. et al 2018 Nat. Phys. 14 1223
- [11] Wan B. et al 2017 Nucl. Fusion 57 102019
- [12] Ding B. J. et al 2011 Phys. Plasma 18 082510
- [13] Liang Y. et al 2013 Phys. Rev. Lett. **110** 235002
- [14] Rack M. *et al* 2014 Nucl. Fusion **54** 064016
- [15] Yao L. H. et al 2001 Nucl. Fusion 41 817
- [16] Li J. et al 2013 Nat. Phys. 9 817

- [17] Wan B. et al Recent advances in EAST physics experiments in support of steady-state operation for ITER and CFETR, 27th IAEA Fusion Energy Conf. OV/2-2 (Gujarat, India, 2018)
- [18] Feng Y. et al 1999 J. Nucl. Mater. 812 266
- [19] EIRENE http://eirene.de
- [20] Reiter D. et al 2005 Fusion Sci. Technol. 47 172
- [21] Xu S. et al 2018 Nucl. Fusion 58, 106008
- [22] Zou X. et al Divertor Power Deposition Control and ELM Mitigation with Supersonic Molecular Beam Injection in the EAST Tokamak, 24th IAEA Fusion Energy Conf. PD/P8-08 (San Diego, CA, 2012)
- [23] Frerichs H. et al 2010 Nucl. Fusion 50 034004
- [24] Huang J. et al 2014 Plasma Phys. Control. Fusion 56 075023
- [25] Zheng X. et al 2013 Plasma Phys. Control. Fusion 55 115010
- [26] Frerichs H. et al 2012 Nucl. Fusion **52** 023001
- [27] Kobayashi M. et al 2015 Nucl. Fusion 55 104021
- [28] Stangeby P. C. 2000 The Plasma Boundary of Magnetic Fusion Devices (Bristol: Institute of Physics Publishing)
- [29] Ding B. J. et al 2016 Nucl. Fusion 57 022022
- [30] Lunt T. et al 2012 Nucl. Fusion 52 054013